Impact of Organic Coating on Soot Angular and Spectral Scattering Properties

Guillaume Lefèvre, Jérôme Yon, Maxime Bouvier, Fengshan Liu, Alexis Coppalle

Environmental Measurements Methods

Impact of organic coating on soot angular and spectral scattering properties

Guillaume Lefevre, Jérôme Yon, Maxime Bouvier, Fengshan Liu, and Alexis Coppalle

Environ. Sci. Technol., **Just Accepted Manuscript** • DOI: 10.1021/acs.est.8b05482 • Publication Date (Web): 06 May 2019

Impact of organic coating on soot angular and spectral scattering properties

Guillaume Lefevre [1], Jérôme Yon [1,], Maxime Bouvier [1], Fengshan Liu[2] and Alexis Coppalle[1]*

[1]Normandie Univ, INSA Rouen, UNIROUEN, CNRS, CORIA, 76000 Rouen, France.

[2]Black Carbon Metrology, National Research Council, Ottawa, Ontario K1A OR6, Canada.

Abstract

In the last two to three decades many efforts have been made to evaluate the radiative properties of soot in flames. Due to the strong impact of soot on global warming and the aging process of soot particles in the atmosphere, it is necessary to gain a better understanding on how the radiative properties of soot are affected by coating with non-absorbing organic aerosol compounds. In the present study, the aging process is experimentally mimicked in laboratory by coating oleic acid onto freshly generated soot particles. The morphological restructuring of soot particles is determined by non-optical techniques for mobility diameter and effective density and by angular light scattering for gyration radius and fractal dimension. Both approaches give results in good agreement. Moreover, spectrally resolved scattering measurements between 500 and 700 nm have been carried out. The experimental data are in satisfactory agreement with

previously published numerical results and enable the validation of a Rayleigh-Debye-Gans theory for Coated Fractal Aggregates (RDG-CFA) that could be integrated in climate models or for the interpretation of scattering based measurements.

Keywords: Soot, coating, restructuring, effective density, RDG-FA

***Corresponding author:** Jérôme Yon (yon@coria.fr).

TOC Art

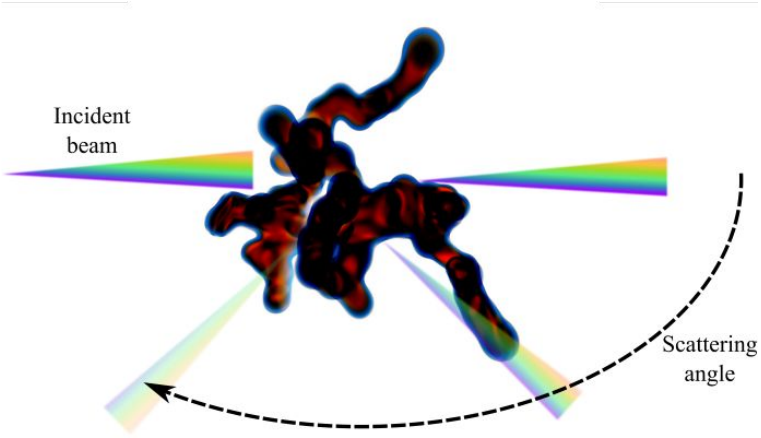

1. Introduction

Due to their black carbon (BC) content, soot particles emitted from various combustion processes (biomass burning [1], transportation [2] etc.) play a major role in the radiative forcing of the Earth. Those particles are known to strongly absorb solar radiation and to influence the process of cloud formation [3]. Soot is considered the second largest anthropogenic contributor to the global warming, just after carbon dioxide [4]. Nevertheless, the quantitative contribution of those particles is subject to many uncertainties caused by the high variability of their radiative properties and uncertainty in BC content. That difficulty is in part related to their complex

morphology. When soot particles are emitted into the atmosphere, semi-volatile organic compounds formed from the photo-oxidation of Volatil Organic Compounds may condense onto freshly emited soot particles. During this aging process, freshly emitted soot particles can be internally mixed with non-absorbing and weakly absorbing atmospheric components to acquire a certain level of coating. This interaction can also cause morphological restructuring modifying the relatively open structure to a more compact one. This effect has been generally observed based on mobility diameter size distribution modification with coating addition [5-11], by determining their mass mobility exponent through effective density measurements [5, 7, 8] or by the determination of the dynamic shape factor χ [9].

The fractal dimension D_f of the particles is a more direct and quantitative way to caracterize the particle morphology and thus restructuring. It can be determined by Transmission Electron Microscopy (TEM) image analysis or alternatively by angular light scattering. Only a few studies have been reported on TEM image analyses of coated soot particles [5, 6, 12]. To our knowledge, angular light scattering has not been applied to coated soot particles. Only Ma, et al. [13] performed multi-angle light scattering measurements of soot aggregates suspended in water, as a proxy of water-coated particles in the aerosol phase.

In general, the organic coating materials of atmospheric relevance are considered non- or weakly-absorbing in the visible and near infrared spectral range. Despite this, the coating plays an important role on the radiative properties of aged particles. Indeed, available studies have confirmed that the absorption and scattering properties are significantly amplified through the "lens effect. Particles coated with organic compounds can double their absorption cross-section compared to that of initially uncoated ones [14-21]. The enhancement appears to be much stronger for scattering with a large range of reported factors from 3.8 [21] to 10 [11]. Soewono

[10] added a coating of oleyl alcohol on carbon nanoparticles produced from a PALAS generator and observed an amplification of scattering by a factor of 2 to 15 for a mass increase due to coating by a factor 1.8 to 5.5, respectively. In consequence, it seems evident that the scattering enhancement is not linearly related to the mass of coating material added to the soot particles and can be significantly stronger than the absorption enhancement.

Although numerous experimental studies have been devoted to quantify the enhancement of absorption and scattering properties of coated soot particles in recent years, unfortunately, the mechanisms of the enhancement are not yet clearly understood. Moreover, there are currently no analytical expressions that could be conveniently used in climate models to provide accurate radiative properties of coated soot particles. Instead, the uniform equivalent sphere model (Mie theory) or the coated equivalent sphere model (Core-Shell-Mie) are still commonly used in climate modeling, in spite of the poor accuracy of such highly simplified models as demonstrated in many recent studies employing exact numerical approaches (T-Matrix [22-25] or Discrete Dipole Approximation [12, 26, 27]). Finally, we can also note that, except the recent work conducted by Lefevre et al. [19] with a focus on the extinction enhancement of soot particles by coating, there have been no experimental studies that performed a direct comparison between measurements and numerical simulations.

In this study, we proposed a generalized Rayleigh-Debye-Gans theory for Fractal Aggregates (RDG-FA) to coated fractal aggregate particles (RDG-CFA) to represent the radiative properties of coated fractal aggregates by simple analytical expressions that could be easily implemented in climate models. RDG-CFA is experimentally evaluated through angular and spectral scattering measurements of soot produced by a miniCAST soot generator and coated with oleic acid. In

addition, the experimental results are compared to the numerical simulation perfomed by Liu et al. [26] for the same coated soot particles.

2. Experimental setup

2.1. Soot generation and coating device

Carbonaceous particles were produced with a commercial soot particle generator (miniCAST 5201C Jing Ltd), which has been extensively used in the literature [19, 28, 29]. In the current study, the considered operation conditions (60 mln/min propane, 0 mln/min mixing nitrogen, 1.5 ln/min of oxidation air, 20 ln/min of dilution air and 7 ln/min of nitrogen quench gas) corresponds to one of the set-points investigated in [19, 28]. The produced soot particles have a very low content of organic compounds (4.1% OC/TC), a mass equivalent primary particle diameter of 29.6 nm, a geometric mean primary particle diameter of $D_{p,\,geo} = 26.6\,nm$, with a geometric standard deviation $\sigma_{geo} = 1.31$, and a bulk density of 1543 kg/m^3 [30].

Once generated, the soot containing aerosol exhaust is further diluted by filtered clean air with a constant flowrate (0.8 ln/min). The diluted exhaust flow is then sent into a coating chamber. This coating device is based on the same design as that of Moteki and Kondo [31] and consists of a bottle (500 mL) partially filled with oleic acid ($\rho^c = 895\,kg.m^{-3}$) and maintained at an adjustable temperature (100-140°C) with an oil bath. It has been shown that the temperature range of the coating device can produce a coating thickness in the range of $e = 0 - 31\,nm$ (see [19] or Section 3.1). The corresponding mass growth factor (*Gfm*) is in the range 1.05 – 4.9. Finally, the aerosol flow containing coated soot particles is sent to different measurement devices.

2.2. Granulometry and effective density

The mobility size distributions were measured by using a Scanning Mobility Particle Sizer (SMPS). All the mobility size distributions were fitted by a lognormal law. The detailed results of mobility size distributions are reported in SI 1.

By coupling a Centrifugal Particle Mass Analyzer (CPMA, Cambustion) with a SMPS, it is possible to determine the power-law relationship between the mobility diameter D_m and the particle mass m. This allows the determination of the mass-mobility exponent D_{fm} and its prefactor a defined in Eq 1. Equivalently, one can define the particle effective density given in Eq 2.

$$m = aD_m^{D_{fm}} \quad \text{Eq 1}$$

$$\rho_{eff} = \frac{6m}{\pi D_m^3} \quad \text{Eq 2}$$

However, because multiply charged particles can be transmitted through the CPMA and SMPS, a deconvolution process described in detail in SI 2 has been applied.

The detailed results of effective density are reported in SI 3.

2.3. Angularly and spectrally resolved static light scattering

The angular light scattering measurement at 532 nm is identical to the one previously performed by Caumont-Prim, et al. [32]. It consists of a motorized bench, a solid-state green continuous laser source electronically chopped, a photomultiplier connected to a lock-in amplifier and some optics. The motorized bench allows the collection of scattered light over the scattering angle range of $\theta = [7° - 161°]$.

This optical bench has also been adapted for the measurement of spectrally resolved scattered light in the wavelength range of 500-700 nm and is schematically depicted in

Figure 1. A spectrally extended continuous laser source (350-1000 nm) (EQ-99-FC LDLS), which is coupled with a beam collimator (Optoprim, RCOL-2-VIS/IR-SMA) and set on a movable angular arm, is used to illuminate the particle stream. The light scattered by the particles is collected by an optical system consisting of two lenses L1 and L2 of focal lengths 20 and 10 cm, respectively, and focused onto a spectrometer (SP-2150i Ropper Princeton Instrument) with a CCD camera (PIMAX4-1024-EM Princeton Instrument). In this experiment, the detection system (spectrometer + camera) is fixed but the light source can be rotated around the axis of the particle stream. The spectrally resolved scattering measurements have been processed at three scattering angles (θ = 7, 20 and 90°). The incident beam diameter at the location of the particle stream is larger than the particle stream diameter in order to avoid any variation of the measurement volume while changing the scattering angle. Because the light source and the detection system are unpolarized, the collected signal corresponds to vertical-vertical polarized cross section (Eq 5) multiplied by $\frac{1+\cos^2\theta}{2}$.

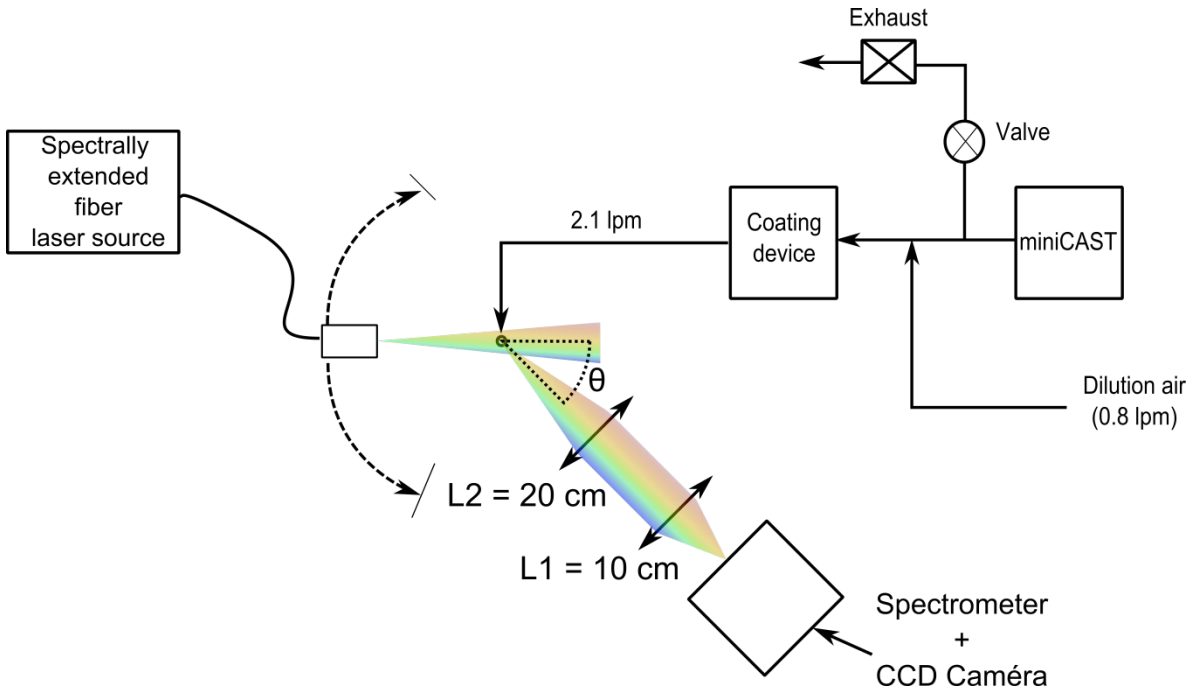

Figure 1 A schematic of the experimental setup - Spectrally resolved scattered light measurement.

The measured signals are calibrated in intensity and interpreted in terms of absolute cross sections. To do this, a protocol based on the 532 nm static light scattering measurements calibrated with size and mass selected polystyrene latex (PSL) spheres (coupling DMA/CPMA) was adopted (more details are given in SI 4).

3. Results and Discussion

3.1. Objective and methodology

As explained in introduction, one of the objectives of this work is to extend the ability of RDG-FA to predict the scattering cross sections of coated soot particles (RDG-CFA). The generalized RDG-FA theory for coated soot particles is presented below, as well as the methodology used for its validation.

152 The fractal dimension D_f and the prefactor k_f are key parameters in the fractal law (Eq 3) to link
153 the aggregate size expressed in gyration radius R_g normalized by the primary particle diameter
154 D_p to the number of primary spheres in an aggregate N_p (related to the particle mass).

$$N_p = k_f\left(\frac{2R_g}{D_p}\right)^{D_f} \quad \text{Eq 3}$$

155 This represents one of the basic assumptions of the RDG theory for Fractal Aggregate (RDG-FA,
156 see [33]) that is expressed in volume in Eq 4 for the determination of the differential scattering
157 cross section $\frac{dC_{vv}}{d\Omega}$ of a fractal particle in the vertical-vertical polarization state :

$$\frac{dC_{vv}}{d\Omega} = A \times (V^t)^2 \frac{9\pi^2 F(m)}{\lambda^4} f(qR_g, D_f) \quad \text{Eq 4}$$

158 In Eq 4, $d\Omega$ represents the differential solid angle, V^t represents the total particle volume, λ is the
159 wavelength, $f(qR_g, D_f)$ represents the structure factor, enabling the description of how light is
160 angularly scattered, and $F(m) = \left|(m^2-1)/m^2+2\right|^2$ represents the scattering function, with m
161 being the refractive index of the bulk material of the primary sphere. $q = \frac{4\pi}{\lambda}\sin\left(\frac{\theta}{2}\right)$ is the norm of
162 the scattering wave vector. In the present study, we used the structure factor proposed in [34]:

$$f = \begin{cases} exp\left(\frac{-(qR_g)^2}{3}\right) if\ (qR_g)^2 \leqslant \frac{3}{2}D_f \\ \left(\frac{3 \quad D_f}{2e(qR_g)^2}\right)^{\frac{D_f}{2}} if\ (qR_g)^2 > \frac{3}{2}D_f \end{cases} \quad \text{Eq 5}$$

163 To generalize the RDG-FA theory to coated fractal aggregates, we first consider the total particle
164 volume V^t to be the sum of the soot core volume V^s and the coating volume V^c. V^s is the product
165 of N_p and the volume of a primary sphere and V^c depends on N_p, the primary sphere diameter D_p
166 , and the coating thickness e. The coating thickness is defined as $e = pD_p$ [26], p denotes the

percentage of coating thickness relative to D_p. Practically, these quantities can be derived from mass measurements using CPMA-DMA) or TEOM as described in [19] and detailed in SI 5. It is also necessary to obtained an effective $F(m)$ that corresponds to the Rayleigh scattering function for a coated primary sphere. This is because the primary spheres are considered uniformly covered with a coating thickness *e*. Thus, we suggest to determine *F(m)* in Eq 4, by interpreting the core-shell Mie scattering cross section of a coated primary sphere by the Rayleigh equivalent scattering function. This will be discussed later.

Finally, parameter A in Eq 4 is a correction factor that has been previously introduced to improve the agreement between the RDG-FA approximation and numerically accurate results, especially to take into account the multiple scattering effects [35, 36] into the RDG-FA formulation. This parameter will be extracted from experimental and numerical results to compare them and to propose an extended RDG-FA theory for accurate modelling of the radiative properties of Coated Fractal Aggregates (RDG-CFA).

3.2. Particle size and morphological restructuring determined by angular light scattering

The angular light scattering pattern is governed by the structure factor (Eq 4), which is dependent on the gyration radius and fractal dimension, two parameters determined by the particle morphology only. For this reason, the angular scattering measurements of coated soot are reported in this section and compared with the results from the SMPS derived experiments.

To our knowledge, the present study is the first one to report such measurements for coated particles. The measured differential angular scattering cross sections ($\frac{dC_{vv}}{d\Omega}$ in Eq 4) for 3 different coating thicknesses at 532 nm are reported in symbols in Fig. 2. We observe an increase of the

differential scattering cross section with increasing the coating thickness. This illustrates the scattering enhancement often attributed to a “lens effect”.

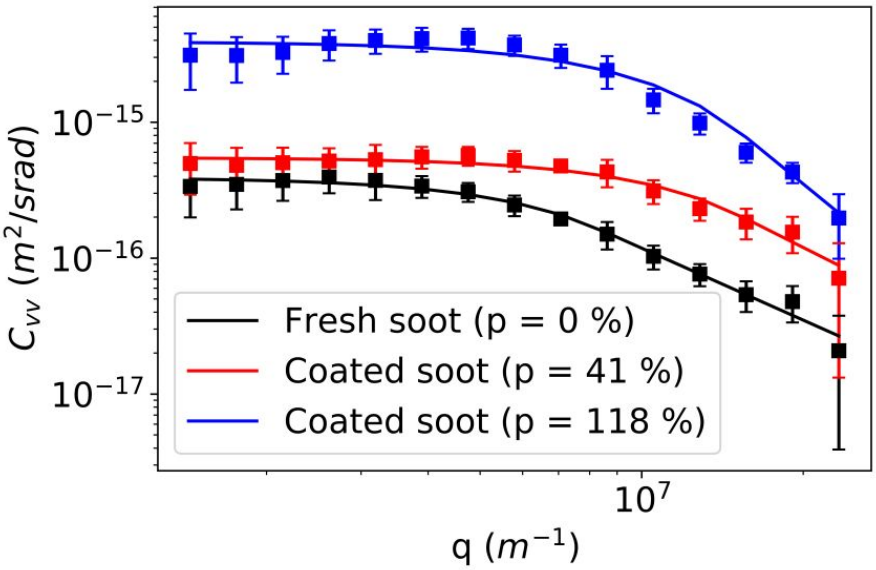

Figure 2 Examples of differential scattering cross sections at different scattering angles at 532 nm (C_{vv}) fitted by the Dobbins and Megaridis structure factor as a function of $q = \frac{4\pi}{\lambda}\sin\left(\frac{\theta}{2}\right)$ for different coating thicknesses.

We now propose to adjust the theoretical expressions given in Eq 4 and Eq 5 based on the angular light scattering experimental results. By this method, an optically derived fractal dimension (D_f) and an equivalent monodisperse gyration radius (R_g) can be determined. Figure 3 shows the fractal dimensions and the gyration diameter obtained optically as a function of the coating thicknesses and their comparison with the results derived from DMA and DMA-CPMA measurements, which are described in SI 1, 2 and 3.

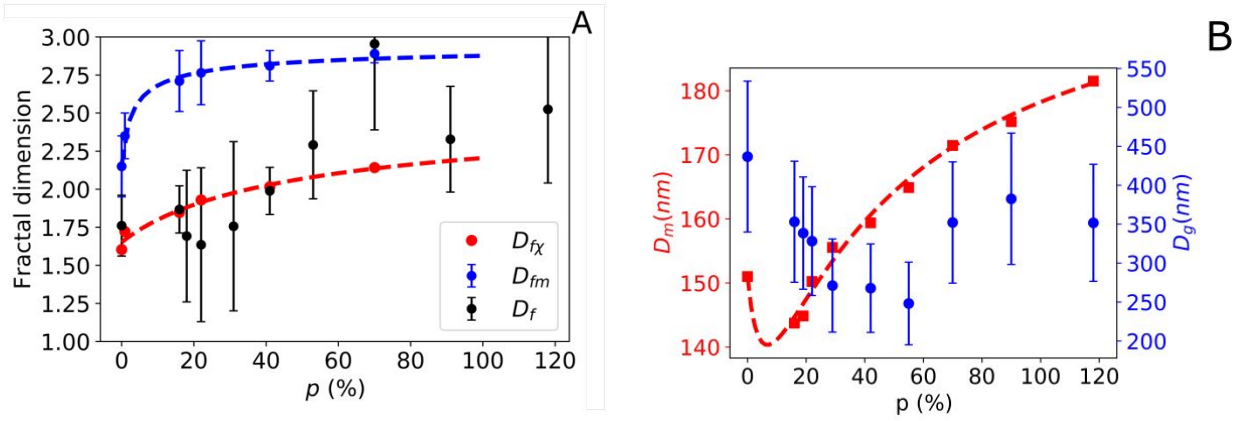

Figure 3 Particle size and morphology determined optically based on angular light scattering measurements for different coating thicknesses. Parameter p represents the percentage of coating thickness relative to the diameter of uncoated soot primary sphere. A: Optically determined fractal dimension D_f, D_{fm} is derived from SMPS/CPMA, $D_{f\chi}$ is derived for shape factor. B: Geometric mean mobility diameter $D_{m,geo}$ (SMPS) and optically determined equivalent monodisperse gyration diameter D_g.

Figure 3-A reports the variation of the optically determined fractal dimension (D_f) with the coating thickness. For comparison, it also reports the scaling exponent based on CPMA-DMA measurements (D_{fm}, whose determination is described in SI 2 and 3, Fig. S5-B) and the fractal dimension of core soot $D_{f\chi}$ determined by interpreting the shape factor (non-optical measurements, whose determination is described in SI 5 and 6).

The proposed quantification of the core soot restructuring shows, through the fractal dimension $D_{f\chi}$, a continuous increase from conventional values without coating (1.6 - 1.7) up to 2.2 for the largest considered coating thickness. This is in good agreement with the TEM image analysis reported by Bambha et al. [5], who observed for ethylene/air diffusion flame soot an increase of the fractal dimension from 1.88 (uncoated) to 2.34 (heavily coated). It is remarkable to observe a

very different behavior of D_f compared to D_{fm} (Fig. 3-A). The core soot compaction does not seem to permit the formation of a very compact spherical cluster $(D_f < 3)$, whereas the coating layer makes the resultant coated particle look like a sphere $(D_{fm} \rightarrow 3)$.

Apart from large discrepancies at p = 22% and 70%, a relatively good agreement is found between $D_{f\chi}$ and D_f ensuring the pertinence of the application of the proposed model detailed in SI 6 for the interpretation of the effective density. This also confirms that the compaction process has not reached a final state for the considered coating thicknesses even if the mass-mobility exponent tends to conclude differently. Also, it appears clear that the mass-mobility exponent is systematically larger than the fractal dimension (after interpretation or optically derived). This is due to the variation of the ratio $2R_g/D_m$ with the particle size as explained in [30, 37].

In figure 3-B, it appears clear that the minimum gyration diameter is observed for larger coating thicknesses ($p \approx 55\%$) than for mobility mean geometric diameter ($p \approx 20\%$). Also, the relative decrease of the representative size parameter is much more significant for gyration radius than for mobility diameter. This illustrates that the mobility diameter is not strongly dependent on morphology and the gyration radius is much more sensitive to the particle restructuring.

3.3. Spectrally resolved light scattering

We report here the experimentally determined spectral scattering properties of coated particles. These results will be used in the next section to validate and compare the results of RDG-CFA theory to numerically accurate DDA results.

Figure 4 reports the measured vertical-vertical differential scattering cross sections in the particular case of uncoated particles (freshly generated core soot) for 3 scattering angles (7, 20 and 90°) over the spectral range of 500-700 nm. In Fig. 4, for comparison, the black dots correspond to the result at 532 nm described in the previous section. As predicted by the

Rayleigh theory, which stipulates that scattering is inversely proportional to the wavelength raised to power 4, a linear increase of the scattering cross section with decreasing wavelength in the log-log plot is observed. However, the slope is not exactly 4 (as indicated in dash lines) due to the angular modulation of the cross section by the structure factor *f* expressed in Eq 5.

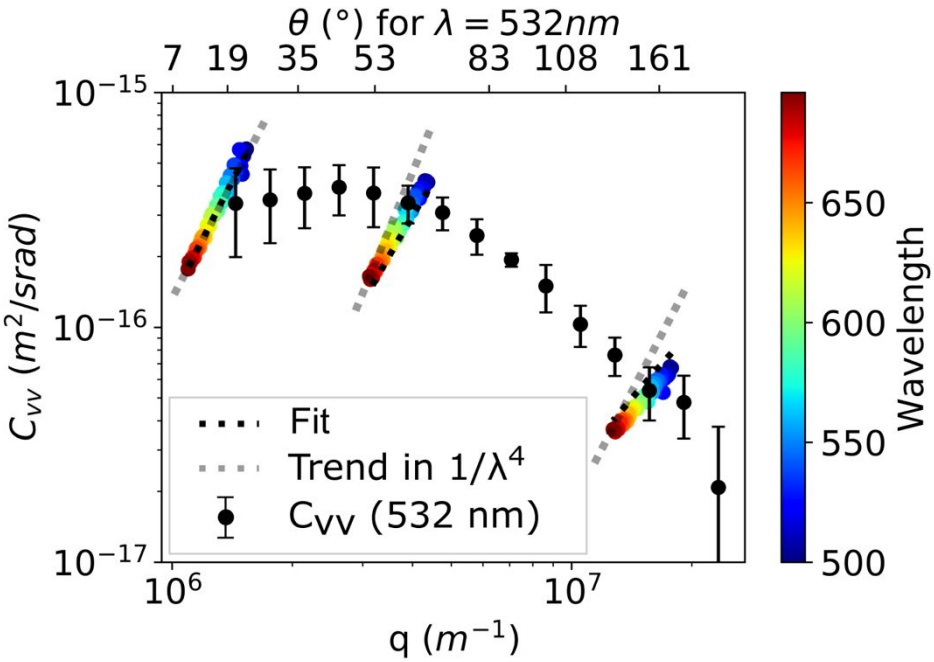

Figure 4 Example of spectrally resolved static light scattering as a function of $q = \frac{4\pi}{\lambda}\sin\left(\frac{\theta}{2}\right)$ for p = 0 % (no coating).

Similar to the model adjustment proposed in the previous section for angular light scattering, we now propose to adjust the model to predict the spectral behavior shown in figure 4. Because both the fractal dimension and gyration radius (previously determined) are independent of wavelength, the only unknown and fitting parameter as a function of wavelength is the forward scattering cross section $C_{vv,0}(\lambda)$:

$$\frac{dC_{vv}(\lambda)}{d\Omega} = \underbrace{C_{vv,0}(\lambda)}_{\substack{research \\ parameter}} f(q, \overbrace{R_g, D_f}^{\substack{Previously \\ determined}}) \qquad \text{Eq 6}$$

It must be noticed that during the current fitting process, the extracted $C_{vv,0}$ is not sensitive to R_g and D_f. Figure 5-A presents the fitted forward scattering cross section (VV) as a function of wavelength for different coating thicknesses. It is evident that the forward scattering is amplified with the increase of coating thickness (except at p = 16%) over the entire spectral range considered. It is also clear that the forward scattering increases with decreasing wavelength, regardless of the coating thickness, which is typical of soot nanoparticles (Rayleigh scattering scales with $1/\lambda^4$). Thus, this phenomenon is preserved even with the addition of coating; however, the spectral dependence seems to deviate from that of uncoated soot particles (decreasing slope with increasing the coating thickness).

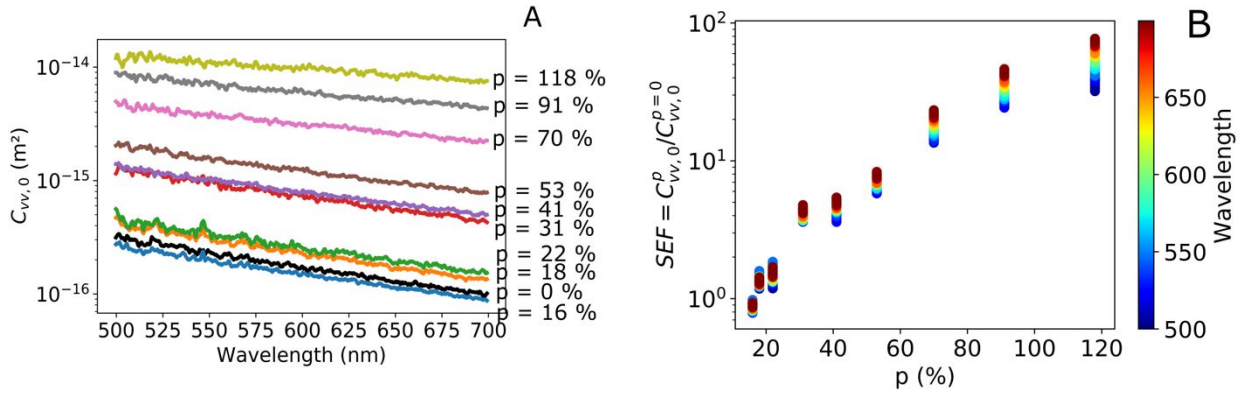

Figure 5 Spectrally resolved forward scattering for different coating thicknesses. A : Forward scattering differential cross section in VV. B: Scattering enhancement (SEF)

Based on equations 4 and 6, the extracted forward scattering cross section is supposed to respect the following theoretical expression:

$$C_{vv,0}(\lambda) = \mathrm{A}(V^t)^2 \frac{9\pi^2 F(m,\lambda)}{\lambda^4} \qquad \text{Eq 7}$$

Thus, the scattering enhancement can be explained not only by the increase of the particle volume (V^t) with coating addition but also by a variation of the Rayleigh based equivalent scattering function $F(m,\lambda)$ and by the correction factor A. However, because the particle volume is independent of wavelength, the spectral dependence of the Scattering Enhancement Factor (SEF), defined here as the ratio of the forward scattering cross section of a coated particle to that of the uncoated one ($SEF = \frac{C_{vv}^{coated}}{C_{vv}^{uncoated}}$, plotted in figure 5-B) can only be attributed to the spectral variation of the product $A \times F(m,\lambda)$ with the coating thickness. It is first observed that the enhancement factor can exceed 10 for coating thicknesses larger than $p > 60$ % as numerically evaluated on the same particles and coating material [26]. We also notice that, the larger the coating thickness is, the stronger the enhancement is at longer wavelengths.

4. Evaluation of the Rayleigh-Debye-Gans theory for Coated Fractal Aggregate: RDG-CFA

A generalized formulation of the RDG-FA theory for coated particles has been proposed in Section 3.1. We aim to evaluate the product $A \times F(m)$ and its dependence on wavelength and coating thickness. To this end, we use the previous results to fix the other parameters in Eq 4 and Eq 5.

For a given coating thickness, the total volume of a coated aggregate can be deduced from its mass (related to a and D_{fm}, reported in Fig. S5) divided by the corresponding density ρ^t (determined and compared with experimental measurements in SI 5). Concerning the gyration radius, we rely on the results of angular light scattering at 532 nm (Fig. 3-B). Concerning the fractal dimension, we consider the one derived from DMA-CPMA measurements ($D_{f\chi}$ in Fig. 3-A), since it is in good agreement with that from the optical measurements and seems more robust

(less experimental uncertainties). Finally, because the aerosol particles are polydisperse, the theoretical cross section given in equations 4 and 5 has to be integrated over the size distribution function determined by the SMPS measurements. This is done by considering a lognormal distribution characterized by the geometric mean mobility diameter and geometric standard deviation reported in SI 1 (Fig. S1). In what follows, the interpolated results (red dash lines in figures S1, 3-A, S5, S9) are considered, the corresponding equations are provided in SI 7.

Due to the previous observations highlighting the spectral dependence of $A \times F(m)$, we propose a two-parameter (AF_{ref},β) dependence through the following equation based on the observed spectral range of 500 nm - 700 nm :

$$A \times F(m,\lambda) = \underbrace{A(\lambda_{ref}) \times F^{CSM}(\lambda_{ref})}_{AF_{ref}} \left(\frac{\lambda}{\lambda_{ref}}\right)^{\beta} \qquad \text{Eq 8}$$

We arbitrarily fix $\lambda_{ref} = 532\ nm$. Thus, AF_{ref} represents the scattering function F^{CSM} at 532 nm modulated by the corresponding multiple scattering correction factor A(λ_{ref}). If β is positive, $A \times F^{CSM}$ increases with λ; Otherwise, it decreases with increasing λ.

Finally, both unknown parameters AF_{ref} and β (in Eq 8) are determined by the least square method to fit the model to the experimentally determined spectrally resolved scattering cross sections measured at the three scattering angles 7, 20, and 90° for each considered wavelength (as illustrated as dotted lines in figure 4). This procedure is repeated for different coating thicknesses.

The results of the least-square fitting are reported in Figs. 6 and 7 in filled circles. In order to evaluate the sensitivity of the fitting to the uncertainties related to different input parameters, a Monte-Carlo error propagation calculation has been conducted. The different input uncertainties

considered are reported in SI 8. The resultant 95% interval confidences are illustrated by the vertical bars.

In the special case of a coated isolated primary sphere ($N_p = 1$), the multiple scattering between primary spheres is absent (A = 1). In this case, $F(m)$ in the proposed RDG-CFA theory should correspond to the Rayleigh equivalent core-shell Mie evaluation $\left(\mathrm{F^{CSM}(m)}\right)$ of the coated primary sphere. The principle is to compute the scattering cross section of a coated primary sphere with the core-shell Mie theory (at 0°) and divide the result by $\pi^4 D_p^6 (1+2p)^6/4\lambda^4$ (Rayleigh theory). For the numerical evaluation, the spectral dependence of the core soot refractive index is taken from Bescond et al. [28] and the refractive index of oleic acid is considered constant ($m_{OA} = 1.4582$). Also, for isolated coated spheres, Eq 8 naturally simplifies to:

$$F^{CSM}(m,\lambda) = F^{CSM}(\lambda_{ref})\left(\frac{\lambda}{\lambda_{ref}}\right)^{\beta^{CSM}} \qquad \text{Eq 9}$$

where $F^{CSM}(\lambda_{ref})$ is reported in Fig. 6-A as the continuous solid curve and β^{CSM} will be discussed later. We observe that the curve decreases rapidly with the coating thickness, especially at relatively low coating thickness up to about 20%, from the $F(m)$ value of the core soot (p = 0%) toward the $F(m)$ value of pure oleic acid (horizontal dotted line) for the largest coating thicknesses considered. These results indicate that, for coating thicknesses large enough, the presence of the primary sphere at the center of a large droplet of oleic acid becomes negligible. The decrease of the effective F^{CSM} seems counter intuitive, since it reveals that the coated primary sphere scattering function ($F(m)$) is reduced with increasing the coating thickness, whereas a global scattering enhancement (even for isolated coated sphere) is observed

and is generally considered as a "lens effect". This highlights the fact that the scattering enhancement is mostly caused by the addition of coating material (increase of V_t).

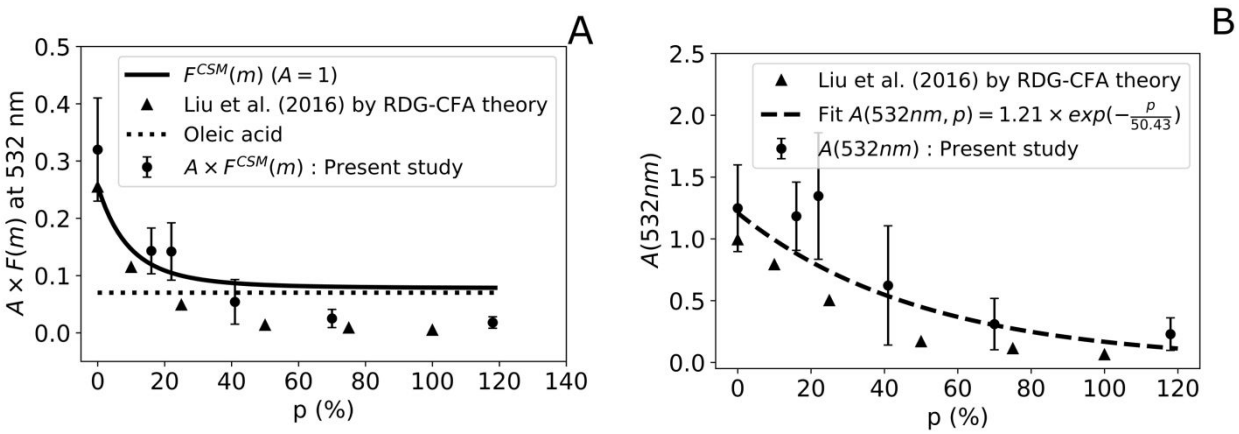

Figure 6 Variation of the effective scattering function at 532 nm modulated by the multiple scattering correction factor with the coating thickness. A : Dependence of scattering function at 532 nm (AF_{ref}) on the coating thickness. B: Evolution of multiple scattering correction factor at 532 nm with the coating thickness.

This behavior is true for isolated primary spheres; however, the interactions among primary spheres in an aggregate make the aggregate total scattering smaller $AF_{ref} < F^{CSM}$, which can be explained by the destructive interferences of scattered light from different coated primary spheres ($N_p > 1$). This is illustrated by the filled circles shown in Fig. 6-A corresponding to the experimental results of this study. Indeed, the product $A \times F^{CSM}(m)$ at 532 nm is shown to decrease toward very small values compared to those from the core-shell Mie approach discussed above. The very small values of the experimental results are reinforced by numerical evaluation. When the numerically determined scattering cross sections for coated aggregates (results given in [26], noting the A parameter in [26] does not correspond to the current A) are interpreted by RDG-CFA, the resultant $A \times F^{CSM}(m)$ at 532 nm (filled triangles in Fig. 6) shows

the same trend as the experimental data and displays a remarkably good accordance. The results shown in Fig. 6-A highlight the good agreement between numerical evaluations based on realistic morphology of coated aggregates and the corresponding experimental results, even though the potential morphological restructuring was not considered in numerical simulations. Finally, the correction factor *A* can be evaluated by dividing the product $A \times F^{CSM}(m)$ at 532 nm by the core-shell Mie equivalent function $F^{\mathrm{CSM}}(m)$ at 532 nm. The experimentally and numerically derived values of *A* are shown in Fig. 6-B as filled circles and filled triangles, respectively. The rapid decrease of $A(532\ nm)$ with increasing the coating thickness highlights the strong influence of coating on the multiple scattering effects. For uncoated soot ($p = 0$ %), one can see that the multiple scattering correction factor at 532 nm can be higher than 1 (about 1.25) in accordance with the literature [35, 38]. It is worth pointing out that this is the first time that the multiple scattering correction factor to RDG-FA is experimentally determined.

The dashed line in Fig. 6-B is an empirically determined exponential fit of *A* to the current experimental results at 532 nm. The corresponding expression is reported in Eq 10 with *p* expressed in %.

$$A(p,\lambda_{ref} = 532nm) = 1.21 \times exp\left(-\frac{p}{50.43}\right) \qquad \text{Eq 10}$$

Figure 7 presents the result of the spectral dependence of the product $A \times F^{CSM}(m)$ on the coating thickness (characterized by the departure of β and β^{CSM} from unity in Eq 8 and Eq 9). Without considering the multiple scattering corrections ($A = 1, N_p = 1$), the core-shell Mie approach predicts a moderate increase of the spectral dependence of $F^{CSM}(m)$ for a thin layer of coating (the plain solid curve that peaks at about p = 15%) followed by a monotonic decay up to an asymptotic value approaching $\beta = 0$ (solid black line). This trend is expected because for sufficiently large coating thicknesses, the scattering function *F(m)* tends towards that of the

coating material (considered independent of the wavelength). A more significant and monotonic increase is observed for β derived from numerical investigation of [26] by considering $A \neq 1$ (filled triangles). The experimental results (filled circles) seem to indicate a much more pronounced spectral dependence than that from the numerical simulation. The error bars are derived from Monte-Carlo error propagation calculations with a 95% interval confidence (see SI 8). The difference between the numerically and experimentally derived β may be explained by the fact that the spectral variation considered for *F(m)* of the core soot in the numerical study of Liu et al. [26] might underestimate the real one (confirmed by their difference for $p = 0$). With increasing the coating thickness, the strong increase of β reveals an increasingly pronounced spectral dependence of the scattered signal. This is an effective way to quantify the observed trend in Fig 5-B.

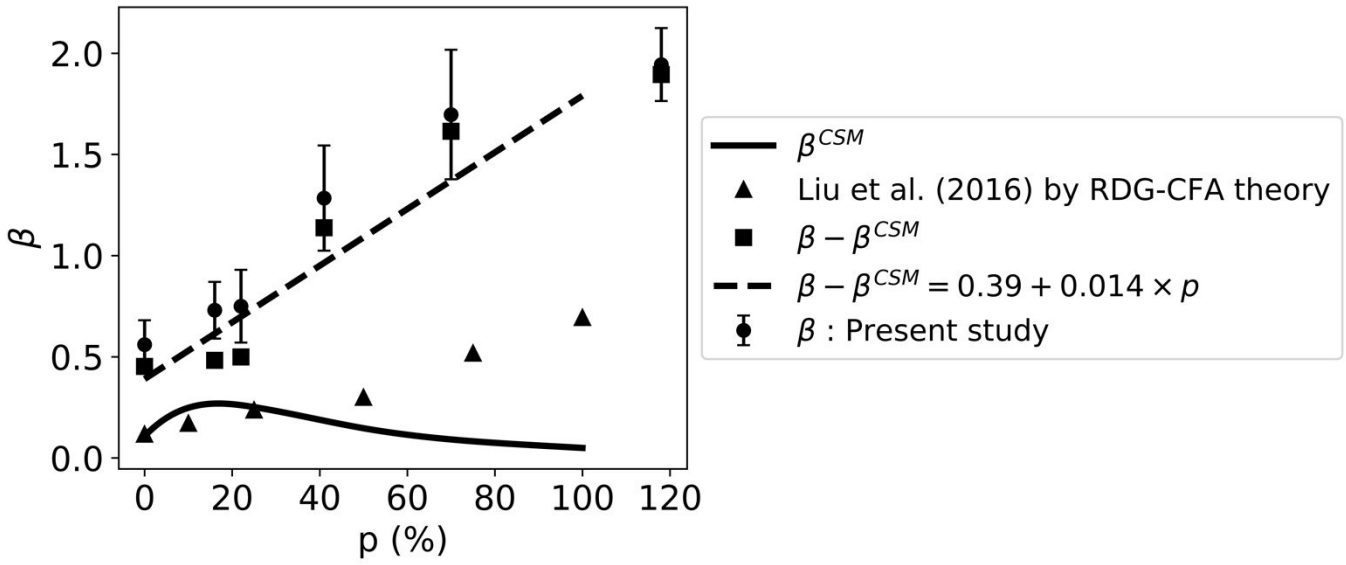

Figure 7 Variation of the spectral dependence of $\beta = A \times F^{CSM}(m)$ with the coating thickness based on experiments, theory, and numerical simulation.

For practical use of the RDG-CFA theory (Eq 4), an empirical expression of the correction factor A was proposed based on the present results reported in Figs 6 and 7. The ratio between equations 8 and 9 leads to:

$$A(p,\lambda) = A(p, \lambda_{ref})\left(\frac{\lambda}{\lambda_{ref}}\right)^{\beta^A(p)} \quad \text{Eq 11}$$

where $A(p, \lambda_{ref})$ is given in Eq 10 and $\beta^{A}(\mathrm{p})$ corresponds to the difference $\beta(\mathrm{p}) - \beta^{\mathrm{CSM}}(\mathrm{p})$, *i.e*, difference in the fitted power of the experimental data and that of spectral dependence of the core-shell Mie Model. We found $\beta^A(p) = 0.39 + 0.014 \times p$ with p expressed in % and $\lambda_{ref} = 532\ nm$.

Nevertheless, this empirical evaluation of $A(p,\lambda)$ is valid for CAST1 soot with oleic acid coating. Additional numerical investigations need to be conducted to further evaluate the robustness of this empirical expression for other configurations.

5. Atmospheric implications

The limitations of Core-Shell Mie for the evaluation of radiative properties of coated soot aggregates have been already shown in previous investigations [12, 26]. In this section, we further illustrate these limitations by comparing the predictions of the Core-Shell Mie approach with the RDG-CFA theory.

Since the total light scattering is an important parameter, in particular for the evaluation of the single scattering albedo, the comparison will be made for the total scattering cross section.

For this comparison, we extrapolate the current results over the wavelength range of 500-1100 nm. The differential scattering cross section is integrated over the entire solid angle to obtain the total scattering cross section.

For the evaluation using Core-Shell Mie, we consider a core sphere having the same volume as the core soot V_s and a shell having the same volume as the coating material volume V_c. The results are reported in Figure 8 that compares the total scattering enhancement factors obtained by Core-Shell Mie and RDG-CFA.

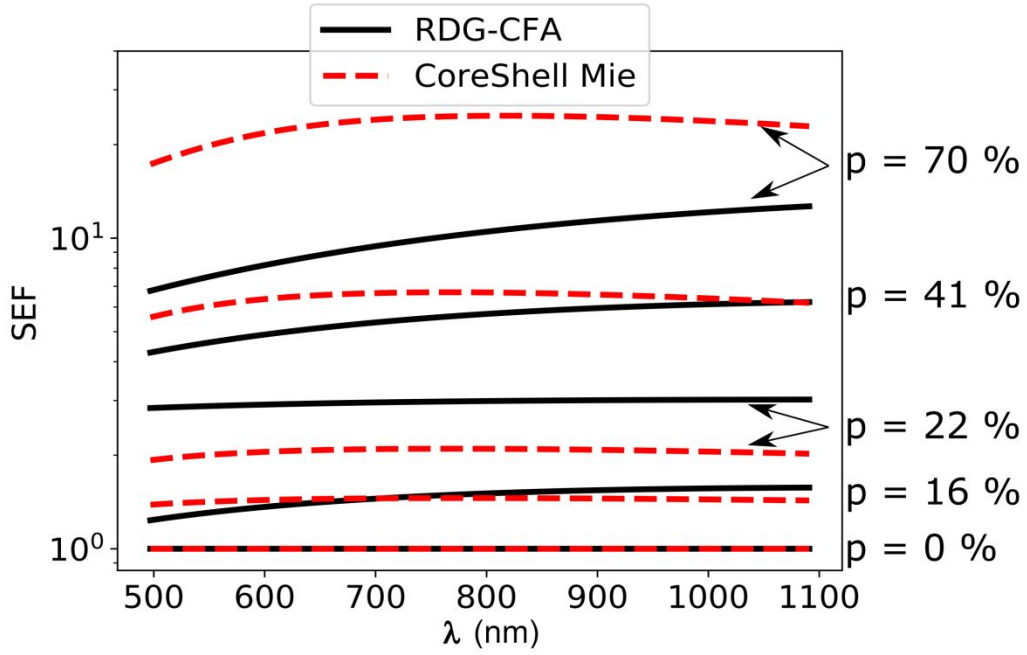

Figure 8 Comparison of the total scattering enhancement factors predicted by the RDG-CFA and Core-Shell Mie theories for CAST1 soot coated with different amount of oleic acid.

As clearly observed in Fig. 8, the Core-Shell Mie model significantly overestimates the total scattering by a factor larger than 2 when the coating thickness is larger than p = 70% (corresponding to a coating layer around the primary spheres about 20 nm). Also, the Core-Shell Mie theory predicts a non-monotonic variation of the enhancement factor with the wavelength

with the peak shifting toward a longer wavelength with increasing the coating thickness. However, this behavior is not observed in the results of the RDG-CFA model.

Extension of the RDG-CFA theory for the absorption cross section of coated aggregates will be investigated as a future study.

Acknowledgements

The project BIOENGINE is co-financed by European Union with the European regional development fund (ERDF) and by the Normandy Regional Council.

Supporting Information

S1. SMPS granulometry results.

S2. Effective density: Measurements and experimental precautions

S3. Effective density: Results

S4. Calibration of Static Light Scattering Measurements

S5. Volume, mass and density of coated aggregates

S6. Soot core fractal dimension determination

S7. Fitted results

S8. Detailed on Monte-Carlo uncertainty analysis

This information is available free of charge via the Internet at http://pubs.acs.org.

References

1. Unger, N.; Bond, T. C.; Wang, J. S.; Koch, D. M.; Menon, S.; Shindell, D. T.; Bauer, S. Attribution of climate forcing to economic sectors. *Proceedings of the National Academy of Sciences* **2010,** *107*, (8), 3382-3387.

2. Kittelson, D. B. Engines and nanoparticles: a review. *J. Aerosol Sci* **1998,** *29*, (5), 575-588.

3. Bond, T. C.; Doherty, S. J.; Fahey, D.; Forster, P.; Berntsen, T.; DeAngelo, B.; Flanner, M.; Ghan, S.; Kärcher, B.; Koch, D. Bounding the role of black carbon in the climate system: A scientific assessment. *J Geophys Res-Atmos* **2013,** *118*, (11), 5380-5552.

4. Jacobson, M. Z. Strong radiative heating due to the mixing state of black carbon in atmospheric aerosols. *Nature* **2001,** *409*, (6821), 695-697.

5. Bambha, R. P.; Dansson, M. A.; Schrader, P. E.; Michelsen, H. A. *Effects of volatile coatings on the morphology and optical detection of combustion-generated black carbon particles*; Sandia National Laboratories (SNL-CA), Livermore, CA (United States): 2013.

6. Ghazi, R.; Olfert, J. Coating mass dependence of soot aggregate restructuring due to coatings of oleic acid and dioctyl sebacate. *Aerosol Science and Technology* **2013,** *47*, (2), 192-200.

7. Schnitzler, E. G.; Dutt, A.; Charbonneau, A. M.; Olfert, J. S.; Jäger, W. Soot Aggregate Restructuring Due to Coatings of Secondary Organic Aerosol Derived from Aromatic Precursors. *Environ. Sci. Technol.* **2014,** *48*, (24), 14309-14316.

8. Schnitzler, E. G.; Gac, J. M.; Jäger, W. Coating surface tension dependence of soot aggregate restructuring. *J. Aerosol Sci* **2017,** *106*, 43-55.

9. Slowik, J. G.; Cross, E. S.; Han, J.-H.; Kolucki, J.; Davidovits, P.; Williams, L. R.; Onasch, T. B.; Jayne, J. T.; Kolb, C. E.; Worsnop, D. R. Measurements of morphology changes of fractal soot particles using coating and denuding experiments: Implications for optical absorption and atmospheric lifetime. *Aerosol Sci. Tech.* **2007,** *41*, (8), 734-750.

10. Soewono, A. Morphology and optical properties of coated aggregates. The University of British Columbia, 2013.

11. Zhang, R.; Khalizov, A. F.; Pagels, J.; Zhang, D.; Xue, H.; McMurry, P. H. Variability in morphology, hygroscopicity, and optical properties of soot aerosols during atmospheric processing. *Proceedings of the National Academy of Sciences* **2008,** *105*, (30), 10291-10296.

12. Adachi, K.; Chung, S. H.; Buseck, P. R. Shapes of soot aerosol particles and implications for their effects on climate. *J Geophys Res-Atmos (1984–2012)* **2010,** *115*, (D15).

13. Ma, X.; Zangmeister, C. D.; Gigault, J.; Mulholland, G. W.; Zachariah, M. R. Soot aggregate restructuring during water processing. *Journal of Aerosol Science* **2013,** *66*, 209-219.

14. Bueno, P. A.; Havey, D. K.; Mulholland, G. W.; Hodges, J. T.; Gillis, K. A.; Dickerson, R. R.; Zachariah, M. R. Photoacoustic measurements of amplification of the absorption cross section for coated soot aerosols. *Aerosol Sci. Tech.* **2011,** *45*, (10), 1217-1230.

15. Cross, E. S.; Onasch, T. B.; Ahern, A.; Wrobel, W.; Slowik, J. G.; Olfert, J.; Lack, D. A.; Massoli, P.; Cappa, C. D.; Schwarz, J. P. Soot particle studies—instrument inter-comparison—project overview. *Aerosol Sci. Tech.* **2010,** *44*, (8), 592-611.

16. Gangl, M.; Kocifaj, M.; Videen, G.; Horvath, H. Light absorption by coated nano-sized carbonaceous particles. *Atmos. Environ.* **2008,** *42*, (11), 2571-2581.

17. Khalizov, A. F.; Xue, H.; Wang, L.; Zheng, J.; Zhang, R. Enhanced light absorption and scattering by carbon soot aerosol internally mixed with sulfuric acid. *J. Phys. Chem. A* **2009,** *113*, (6), 1066-1074.

18. Lack, D. A.; Cappa, C. D.; Cross, E. S.; Massoli, P.; Ahern, A. T.; Davidovits, P.; Onasch, T. B. Absorption enhancement of coated absorbing aerosols: Validation of the photo-acoustic technique for measuring the enhancement. *Aerosol Sci. Tech.* **2009,** *43*, (10), 1006-1012.

19. Lefevre, G.; Yon, J.; Liu, F.; Coppalle, A. Spectrally resolved light extinction enhancement of coated soot particles. *Atmos. Environ.* **2018,** *186*, 89-101.

20. Shiraiwa, M.; Kondo, Y.; Iwamoto, T.; Kita, K. Amplification of light absorption of black carbon by organic coating. *Aerosol Sci. Tech.* **2010,** *44*, (1), 46-54.

21. Xue, H.; Khalizov, A. F.; Wang, L.; Zheng, J.; Zhang, R. Effects of dicarboxylic acid coating on the optical properties of soot. *Phys. Chem. Chem. Phys.* **2009,** *11*, (36), 7869-7875.

22. Liu, C.; Panetta, R. L.; Yang, P. The influence of water coating on the optical scattering properties of fractal soot aggregates. *Aerosol Sci. Tech.* **2012,** *46*, (1), 31-43.

23. Wu, Y.; Cheng, T.; Gu, X.; Zheng, L.; Chen, H.; Xu, H. The single scattering properties of soot aggregates with concentric core–shell spherical monomers. *J. Quant. Spectrosc. Radiat. Transfer* **2014,** *135*, 9-19.

24. Wu, Y.; Cheng, T.; Zheng, L.; Chen, H. Models for the optical simulations of fractal aggregated soot particles thinly coated with non-absorbing aerosols. *J. Quant. Spectrosc. Radiat. Transfer* **2016,** *182*, 1-11.

25. Yin, J.; Liu, L. Influence of complex component and particle polydispersity on radiative properties of soot aggregate in atmosphere. *J. Quant. Spectrosc. Radiat. Transfer* **2010,** *111*, (14), 2115-2126.

26. Liu, F.; Yon, J.; Bescond, A. On the radiative properties of soot aggregates–Part 2: Effects of coating. *J. Quant. Spectrosc. Radiat. Transfer* **2016,** *172*, 134-145.

27. Soewono, A.; Rogak, S. N. Morphology and optical properties of numerically simulated soot aggregates. *Aerosol Sci. Tech.* **2013,** *47*, (3), 267-274.

28. Bescond, A.; Yon, J.; Ouf, F.-X.; Rozé, C.; Coppalle, A.; Parent, P.; Ferry, D.; Laffon, C. Soot optical properties determined by analyzing extinction spectra in the visible near-UV: Toward an optical speciation according to constituents and structure. *J. Aerosol Sci* **2016,** *101*, 118-132.

29. Moore, R. H.; Ziemba, L. D.; Dutcher, D.; Beyersdorf, A. J.; Chan, K.; Crumeyrolle, S.; Raymond, T. M.; Thornhill, K. L.; Winstead, E. L.; Anderson, B. E. Mapping the operation of the miniature combustion aerosol standard (Mini-CAST) soot generator. *Aerosol Sci. Tech.* **2014,** *48*, (5), 467-479.

30. Yon, J.; Bescond, A.; Ouf, F.-X. A simple semi-empirical model for effective density measurements of fractal aggregates. *J. Aerosol Sci* **2015,** *87*, 28-37.

31. Moteki, N.; Kondo, Y. Effects of mixing state on black carbon measurements by laser-induced incandescence. *Aerosol Sci. Tech.* **2007,** *41*, (4), 398-417.

32. Caumont-Prim, C.; Yon, J.; Coppalle, A.; Ouf, F.-X.; Ren, K. F. Measurement of aggregates' size distribution by angular light scattering. *J. Quant. Spectrosc. Radiat. Transfer* **2013,** *126*, 140-149.

33. Sorensen, C. Light scattering by fractal aggregates: a review. *Aerosol Sci. Tech.* **2001,** *35*, (2), 648-687.

34. Dobbins, R. A.; Megaridis, C. M. Absorption and scattering of light by polydisperse aggregates. *Appl. Opt.* **1991,** *30*, (33), 4747-4754.

35. Yon, J.; Liu, F.; Bescond, A.; Caumont-Prim, C.; Rozé, C.; Ouf, F.; Coppalle, A. Effects of multiple scattering on radiative properties of soot fractal aggregates. *J. Quant. Spectrosc. Radiat. Transfer* **2014,** *133*, 374-381.

36. Yon, J.; Liu, F.; Morán, J.; Fuentes, A. Impact of the primary particle polydispersity on the radiative properties of soot aggregates. *Proceedings of the Combustion Institute* **2018,** *37*, (1), 1151-1159.

37. Sorensen, C. The mobility of fractal aggregates: a review. *Aerosol Sci. Tech.* **2011,** *45*, (7), 765-779.

38. Sorensen, C. M.; Yon, J.; Liu, F.; Maughan, J.; Heinson, W. R.; Berg, M. J. Light Scattering and Absorption by Fractal Aggregates Including Soot. *J. Quant. Spectrosc. Radiat. Transfer* **2018,** *217*, 459-473.